EVALUATING STATIC AND DYNAMIC IMPACTS OF GEOMAGNETIC DISTURBANCES ON INTERCONNECTED POWER GRIDS

A Thesis

by

YIQIU ZHANG

Submitted to the Office of Graduate and Professional Studies of
Texas A&M University
in partial fulfillment of the requirements for the degree of

MASTER OF SCIENCE

Chair of Committee,	Thomas Overbye
Committee Members,	Timothy Davis
	Robert Nevels
	Le Xie
Head of Department,	Miroslav Begovic

May 2019

Major Subject: Electrical Engineering

ABSTRACT

Geomagnetic disturbances (GMDs) can potentially impose operational challenges on power systems and cause damage to essential grid assets through geomagnetically induced currents (GICs). Therefore, to maintain power system efficiency and reliability, it is essential to study how GMDs impact power systems. This work contains two separate research topics related to GMDs. The first research topic is associated with a spatially non-uniform GMD event called localized geomagnetic field enhancement. Characterized by geomagnetic fields substantially increasing in some areas, localized geomagnetic field enhancements cause the localized augmentation of geoelectric fields and flow of "extra" GICs in power grids. Considering that the distribution of the "extra" GICs directly affects the planning and operations of the grids, this work utilizes the superposition principle and defines a sensitivity associated with the "extra" GICs to study the impact scopes of localized geomagnetic field enhancements. Sensitivity analysis is performed on a small 20-bus benchmark system and a large 10k-bus synthetic network, respectively. The results show that the impact scope of a square localized geomagnetic field enhancement area is generally less than one and a half times its width. In other words, the "extra" GICs are localized. The second research topic focuses on studying the impacts of GMDs/GICs on power system transient stability under different contingent conditions. In the work, various contingencies are applied to the 10k-bus synthetic network individually in the presence of time-invariant GMDs, while the changes in the transient stability margin are evaluated using different metrics. Several case studies are presented as examples of the potential

effects of GMDs. The results show that GMDs can alter power system transient margin. Therefore, this work suggests that relevant transient stability studies may need to be conducted to ensure secure power system operations under the effect of GMDs.

ACKNOWLEDGEMENTS

First, I would like to thank my supervisor, Dr. Overbye, for providing me opportunities to work on fascinating research topics and to work with a group of intelligent and enthusiastic people. Under his mentorship, my knowledge and passion for power systems has extensively grown. I feel very honored and fortunate to have been working with him through my time at Texas A&M University.

I would also like to thank my family and my boyfriend, Minhao, for listening to me problems and encouraging me in all of my pursuits. I am especially grateful to my parents who have been supporting me, believing in me, and wanting the best for me. This journey would not have been possible without the support of them.

CONTRIBUTORS AND FUNDING SOURCES

I would like to thank Professors Thomas Overbye, Robert Nevels, Le Xie of the Department of Electrical and Computer Engineering and Professor Timothy Davis of the Department of Computer Science and Engineering for serving on my M.S. defense committee.

I would like to acknowledge my colleagues Komal Shetye, Raymund Lee, Dr. Adam Birchfield, and my supervisor Dr. Thomas Overbye for their technical guidance.

I would also like to acknowledge the National Science Foundation (NSF) for primarily funding my research and master's education under Award Number NSF 15-20864.

TABLE OF CONTENTS

Page

LIST OF FIGURES

Page

LIST OF TABLES

Page

CHAPTER I

INTRODUCTION

Geomagnetic disturbance (GMD) is an emerging topic in the electric power industry, given that it has the potential to cause great challenges on system operations and damage to grid assets. Detrimental effects of GMDs on power systems can be seen in the well-known March 13, 1989 GMD in the North America that led to a 9-hour blackout of Hydro-Quebec [1].

Naturally occurring GMDs are usually caused by solar coronal mass ejections (CMEs). During a CME, a massive amount of charged particles are ejected from the sun's surface. Carried by the solar wind, the particles sometimes travel toward the earth and instigate fluctuations in the earth's magnetic fields [2], [3]. The disturbed magnetic fields will generate slowly-varying electric fields with frequencies in a range between 0.01 Hz and 0.5 Hz at ground level [2]. The quasi-dc geoelectric fields then induce dc voltages across transmission lines and cause geomagnetically induced currents (GICs) to flow in the transmission lines that are connected to wye-grounded transformers [2], [3]. With the imposition of dc-offsets (i.e. GICs) on the transformers' ac waveforms, the transformers may experience saturation every half cycle. The direct effects of the transformer half-cycle saturation are increased harmonic currents, increased reactive power absorption, and internal localized heating in transformers [2]-[6]. The potential consequences corresponding to each of the direct effects are protection device maloperations, voltage collapse, and irreversible damage to the transformers [2]-[6].

To get bulk electric systems in North America prepared for GMDs, many research efforts and resources have been devoted to assessing and preventing the negative impacts of GMDs. For the same reason, this work is dedicated to studying two research topics related to GMDs (1) examining the GIC distribution during a spatially non-uniform GMD event called localized geomagnetic field enhancement (2) investigating the impact of GMDs on power system transient stability margin. The studies associated with these two separate research topics are presented in CHAPTER I and CHAPTER II, respectively.

CHAPTER II

GRID IMPACT EVALUATION OF LOCALIZED GEOMAGNETIC FIELD ENHANCEMENTS USING SENSITIVITY ANALYSIS

Background

A. Description of Localized Geomagnetic Field Enhancements

During a localized geomagnetic field enhancement, the resulting geoelectric field in an area on the order of a few hundreds of kilometers or less has a magnitude much higher than those at neighboring areas [7], [8]. Fig.1 from [8] provides spatial and magnitude scales for a localized field enhancement and the geoelectric fields at its neighboring areas.

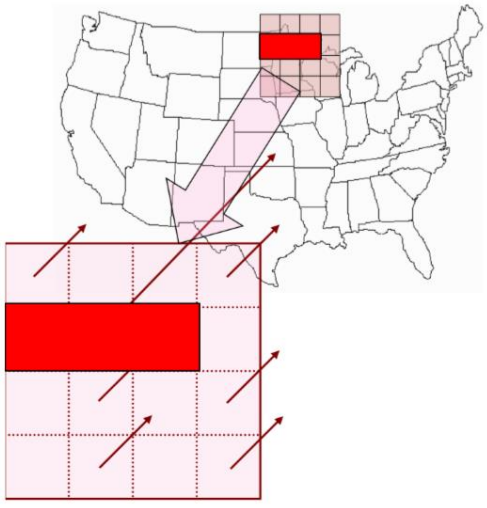

Fig.1. A localized field enhancement and the geoelectric fields at its neighboring areas are indicated by the red rectangle and pink squares, respectively. The directions of the arrows show the fields' orientations, while the lengths are proportional to the fields' magnitudes. Reprinted from [8].

The increase in the geoelectric field strength then induces "extra" GICs to flow across transmission lines, which directly affects the planning and operations of power grids. Therefore, it is necessary to develop a methodology to quantify the impact scopes of localized field enhancements.

B. Literature Review and Proposed Methodology Overview

The impact scope of the "extra" GICs due to localized geomagnetic field enhancements has not been assessed quantitatively in previous works. Without the localized field enhancements considered, earlier works such as [9] and [10] suggested that GICs are localized. Reference [8] illustrated the regional impact of a localized field enhancement by statistically showing that only a small set of transformers experience notable changes in GICs in the presence of a localized field enhancement. Moreover, the case study in [11] exhibited a negative correlation between the distance from a transformer to a localized field enhancement and the change in GIC experienced by the transformer.

As the application of linear superposition in GIC modeling is justified in [11], [12], this work decomposes a localized enhanced geoelectric field into a base field and an "extra" field. A sensitivity associated with the "extra" GICs is defined and utilized to quantify the impact of the localized field enhancement on transformers. The results from sensitivity analyses, performed on a small 20-bus benchmark system [13] and a large 10k-bus synthetic network [14]-[16] show that "extra" GICs are localized. To be specific, the

results suggest that the impact scope of a square localized field enhancement area is generally less than one and a half times its width.

C. GIC Modeling Overview

This section gives an overview of the GIC calculation used here [10], [17], [9]. Consider a power system containing b buses, s substations, m transmission lines, and r transformers. Let N equal to the sum of b and s. Therefore, the system has N nodes in total which comprise b buses and s substation neutrals. The nodal voltage vector **V** can be found by using

$$\mathbf{V} = \mathbf{G}^{-1}\,\mathbf{I}. \tag{1}$$

where **G** is an N-dimensional symmetric matrix resembling the bus admittance matrix but altered to account for substation neutral buses and substation grounding resistances; **I** is an N-dimensional vector with each entry holding the value of the Norton equivalent dc current injection at the corresponding node [17], [9], [18].

According to [19], the GMD induced voltage across line *m*, symbolized as U_m, can be determined by integrating the geoelectric field along the route of line *m*

$$U_m = \int_{\mathrm{R}} \vec{E}_m \cdot d\vec{l}_m \tag{2}$$

where $\bar{E}_m$ is the geoelectric field in the line segment $d\bar{l}_m$ and R represents the geographic path of line m. In this study, a variable with a bar on its top denotes a vector. In the case of a uniform geoelectric field, (2) is equivalent to

$$U_m = E_m L_m \cos(\theta_{E,m} - \theta_{L,m}) \tag{3}$$

where E_m and $\theta_{E,m}$ represent the magnitude (V/km) and direction of the geoelectric field in line m; L_m and $\theta_{L,m}$ represent the length and the direction of line m ("from" bus – "to" bus). In this study, all the directions are defined in degrees and referred to the north. The Norton current injection at bus b can be determined by solving

$$I_b = \sum_{m=1}^{H} I_m = \sum_{m=1}^{H} g_m U_m = \sum_{m=1}^{H} g_m L_m \cos(\theta_{E,m} - \theta_{L,m}) E_m \tag{4}$$

where I_m is the Norton current injection contributed by line m from a set of lines with direct connections to bus b (The set contains H lines.); g_m is the three-phase conductance of line m (in siemens); the total Norton current injection at bus b, I_b, equals the sum of the Norton current injections (I_m) contributed by the H lines [11], [18]. As for the substation neutrals, since they are not directly connected to any lines, their Norton current injections are all zeros [18]. According to (4), (1) can be modified as

$$\mathbf{V} = \mathbf{G}^{-1}\,\mathbf{B}\,\mathbf{A}\,\mathbf{E} \tag{5}$$

where **E** is an m-dimensional vector with entry *m* equal to the magnitude of the geoelectric field in line *m*; **A** is an m-dimensional diagonal matrix with its diagonal entry *m* equal to the cosine of the angle difference between the geoelectric field and line *m*; **B** is an N-by-m matrix where column *m* is associated with line *m* and only has non-zero values in the rows corresponding to the "from" and "to" buses of line *m*; each non-zero entry in **B** has a magnitude equal to the product of the three-phase conductance and length of the associated line and follows the sign convention that a positive sign (a negative sign) is assigned to a "from" bus entry ("to" bus entry) [17], [9], [18]. Based on Ohm's law, GIC flowing through any connections can be obtained by using

$$I_{GIC,i,j} = g_{i,j}\,(V_i - V_j) \tag{6}$$

where V_i and V_j are the voltages at node *i* and *j*, respectively; $g_{i,j}$ represents the per-phase conductance of the connection between nodes *i* and *j*; $I_{GIC,i,j}$ represents the GIC flowing through the connection [9], [11], [18].

GICs participate in the power flow as additional reactive loads on transformers which are assumed to vary linearly with the "effective" GICs of the transformers. The effective GIC of transformer *r* is defined as

$$I_{Eff,r} = | I_{GICH,r} + \frac{I_{GICL,r}}{a_{t,r}} | \quad (7)$$

where $I_{GICH,r}$ and $I_{GICL,r}$ are the per-phase GICs flowing into the high side winding (or the series winding of an autotransformer) and low side winding (or the common winding) of transformer r, respectively; $a_{t,r}$ is the turns ratio of transformer r [20], [17], [9], [18]. In combination with (5), the effective GIC of transformer r can be determined from the nodal voltages using a row vector $\mathbf{C}_r$

$$I_{Eff,r} = | \mathbf{C}_r \mathbf{V} | = | \mathbf{C}_r \mathbf{G}^{-1} \mathbf{B} \mathbf{A} \mathbf{E} | \quad (8)$$

where $\mathbf{C}_r$ is an N-dimensional row vector. $\mathbf{C}_r$ is sparse and only has non-zero values at entries associated with transformer r's primary winding, secondary winding, and substation neutral [9], [18]. Equation (8) shows that the linearity is preserved for the product of $\mathbf{C}_r$ and (5), considering that the linearity of (5) has been proved in [11] and the matrix multiplication of $\mathbf{C}_r$ and (5) is essentially a linear operation. For simple reference in the later text, define

$$I_{AEff,r} = \mathbf{C}_r \mathbf{V} = \mathbf{C}_r \mathbf{G}^{-1} \mathbf{B} \mathbf{A} \mathbf{E} \quad (9)$$

where $I_{AEff,r}$ is the "actual effective GIC" of transformer r. The principle of superposition can be applied to any linear operations involving $I_{AEff,r}$.

Proposed Methodology

A. Derivation of Localized Field Enhancement Associated Sensitivity

A uniform geoelectric field cannot be assumed in the presence of a localized field enhancement, since the geoelectric field inside the localized field enhancement area is higher in magnitude and even has a different direction than that in the surrounding areas. In this case, the GMD-induced dc voltage across each line can be estimated by summing the segment-wise GMD-induced voltages due to different fields, under the assumption that the field in each segment is uniform [9].

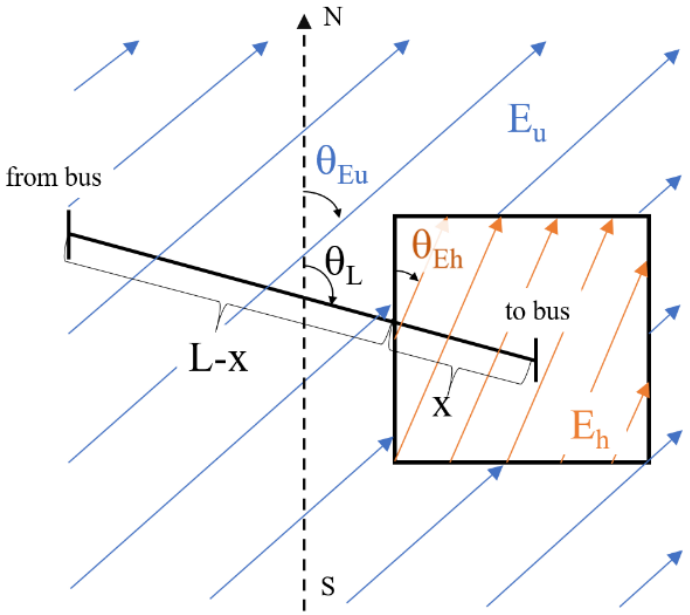

Fig.2. An L km long transmission line with x km long segment falling inside a localized field enhancement area, indicated by the rectangle. The magnitudes and directions of the geoelectric fields inside and outside the area are indicated by the densities and orientations of the orange and blue arrows, respectively.

Refer to Fig.2 and consider a scenario where line m of L_m km and $\theta_{L,m}$ degrees was originally in a uniform geoelectric field of $E_{u,m}$ V/km and $\theta_{Eu,m}$ degrees. The GMD-induced dc voltage in line m, $U_{u,m}$, can be obtained by solving

$$U_{u,m} = \bar{E}_{u,m} \cdot \bar{L}_m \tag{10}$$

where $\bar{E}_{u,m}$ and $\bar{L}_m$ represent the uniform geoelectric field and line m in vector notation. Then, a localized field enhancement occurs and the geoelectric field inside the localized enhancement area changes to $E_{h,m}$ V/km and $\theta_{Eh,m}$ degrees. The segment of line m residing within the localized field enhancement area has a length of x km. Based on [9] and [11], now the GMD-induced dc voltage in line m changes to

$$U_{n,m} = \bar{E}_{u,m} \cdot (\bar{L}_m - \bar{x}_m) + \bar{E}_{h,m} \cdot \bar{x}_m \tag{11}$$

where $U_{n,m}$ is the new GMD-induced dc voltage across line m; $\bar{x}_m$ denotes the segment residing within the localized field enhancement area. To facilitate the derivation, define

$$\bar{E}_{c,m} = \bar{E}_{h,m} - \bar{E}_{u,m} \tag{12}$$

where $\bar{E}_{c,m}$ is the vector notation of the change in the geoelectric field due to the localized field enhancement and will be referred as the "extra" field. The extra voltage source across

line m, ΔU_m, induced solely by the extra field can be obtained by subtracting (10) from (11) gives

$$\Delta U_m = \vec{E}_{c,m} \cdot \vec{x}_m = E_{c,m}\, x_m \cos(\theta_{Ec,m} - \theta_{L,m}) \tag{13}$$

where $E_{c,m}$ and $\theta_{Ec,m}$ are the magnitude and direction of the extra field in line m. Since [11] has justified that the total GIC induced in a transmission line by multiple geoelectric fields equals to the combination of the GICs induced by each individual geoelectric field, the GIC flowing in line m equals to the sum of the GICs induced respectively by the extra field and base field. Given (9) and (13), the change in the actual effective GIC for transformer r can be determined by solving

$$\Delta I_{AEff,r} = \mathbf{C}_r\, \mathbf{\Delta V} = \mathbf{C}_r\, \mathbf{G}^{-1}\, \mathbf{B}\, \mathbf{\Sigma}\, \mathbf{A}_c\, \mathbf{E}_c \tag{14}$$

where $\Delta I_{AEff,r}$ is the extra actual effective GIC for transformer r caused by the extra field, which will be referred to as EAE_r; $\mathbf{\Sigma}$ is an m-dimensional diagonal matrix with entry m on the diagonal equal to the fraction of the length of line m falling inside the localized field enhancement area; $\mathbf{A}_c$ is an m-dimensional diagonal matrix with its diagonal entry m equal to the cosine of the angle difference between the extra field and line m; $\mathbf{E}_c$ is an m-dimensional vector with entry m equal to the magnitude of the extra field in line m. For simplicity of notation, define the following row vector for transformer r

$$\frac{d\Delta I_{AEff,r}}{d\mathbf{E}_{c,T}} = \mathbf{C}_r \mathbf{G}^{-1} \mathbf{B} \boldsymbol{\Sigma} = \mathbf{S}_{c,T,r} \tag{15}$$

where $\mathbf{E}_{c,T}$ is an m-dimensional vector with entry m equal to the magnitude of the extra field tangent to line m; $\mathbf{S}_{c,T,r}$ is an m-dimensional row vector with entry m equal to EAE_r with 1 V/km variation in the extra field tangent to line m. In combination of (15), (14) can be transformed into a summation form

$$\Delta I_{AEff,r} = \mathbf{S}_{c,T,r} \mathbf{A}_c \mathbf{E}_c = \sum_{m=1}^{m} (\mathbf{S}_{c,T,r}[m] \cos(\theta_{Ec,m} - \theta_{L,m}) E_{c,m}) \tag{16}$$

where $\mathbf{S}_{c,T,r}[m]$ represents entry m in $\mathbf{S}_{c,T,r}$. Under the assumption that the extra field is uniform in magnitude within the localized field enhancement area, the sensitivity used to quantify the impact of the localized field enhancement on transformer r can be defined as

$$\frac{d\Delta I_{AEff,r}}{dE_c} = \sum_{m=1}^{m} (\mathbf{S}_{c,T,r}[m] \cos(\theta_{Ec,m} - \theta_{L,m})). \tag{17}$$

where E_c represents the magnitude (assumed uniform) of the extra field. The sensitivity defined in (17) will be referred to as SEAE (sensitivity of the extra actual effective GIC of a transformer). When the extra field is 1 V/km, SEAE of a transformer equals the sum of the EAEs contributed by each individual line. To account for an extra field with a nonuniform magnitude, scaling factors can be combined with corresponding summation

terms in (17) as multipliers of the assumed extra field magnitude. In the worst-case scenario, SEAE for transformer *r* can be written as

$$\frac{d\Delta I_{AEff,wc,r}}{dE_c} = \sum_{m=1}^{\mathrm{m}} | \mathbf{S}_{c,T,r}[m] |. \tag{18}$$

The worst-case scenario occurs when a nonuniform extra field (nonuniform in terms of direction) is aligned with every line segment residing within the localized field enhancement area. Regardless of the likelihood of the worst-case scenario, the worst-case SEAE is used as the upper limit of SEAE when the consideration of angle differences is not preferred. During a localized field enhancement, the effective GIC of transformer *r* can be determined by using superposition

$$I_{Eff,r,n} = | I_{AEff,r,u} + \Delta I_{AEff,r} | \tag{19}$$

where $I_{Eff,r,n}$ represents the effective GIC of transformer *r*; $I_{AEff,r,u}$ is the part of the actual effective GIC contributed by the base field; $\Delta I_{AEff,r}$, or EAE_r, is the part of the actual effective GIC contributed by the extra field. Equation (19) can be further generalized to account for multiple localized field enhancements by adding more $\Delta I_{AEff,r}$ terms associated with different localized enhancements. Moreover, SEAEs can be determined to facilitate the calculation of the effective GICs. Thus, equation (19) provides a flexible and prompt

way of analyzing the impact of localized field enhancements by decoupling the impact of the base field and that of the extra field.

Localized Geomagnetic Field Enhancement Case Studies

A. 20-bus Benchmark System

In this section, a localized field enhancement impact study is conducted on a 20-bus benchmark system [13]. The SEAEs for two selected transformers are determined as functions of the extra field's angle.

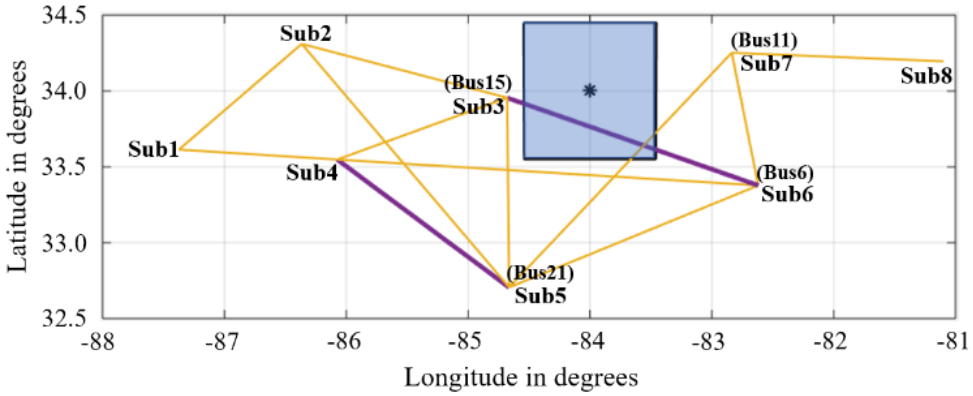

Fig.3. A geographic view of a 20-bus system with the shaded area indicating the location of the localized field enhancement area. The locations of all substations and some buses of interest (in parentheses) are shown.

A geographic view of the 20-bus system is shown in Fig.3. The yellow lines and purple lines represent the single-circuit lines and double-circuit lines, respectively. A localized field enhancement occurs in a 100 km by 100 km area, indicated by the shaded rectangle centered at (34º N, 84º W). Assume that a uniform base geoelectric field of 1

V/km is applied to the footprint shown in Fig.3, except the localized field enhancement area. The geoelectric field inside the localized field enhancement area has a magnitude of 2 V/km and the same direction of the base field. The base field and localized enhancement field are rotated simultaneously from 0 to 360 degrees in increments of 10 degrees so that the extra field is always 1 V/km in the same direction as the base field.

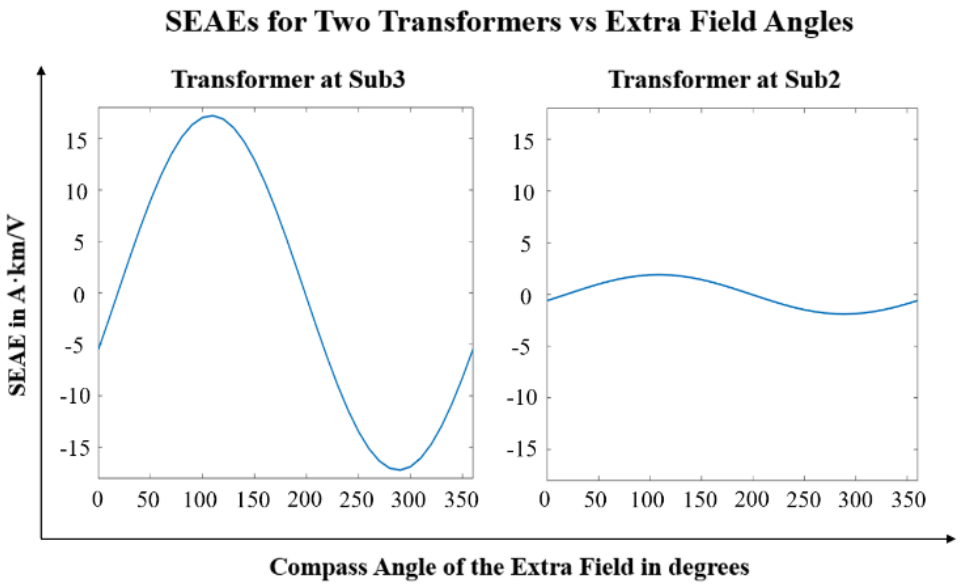

Fig.4. The variation in SEAE for the transformer at substation 3 and transformer at substation 2 as the 1 V/km extra field varies from 0 to 360 degrees in steps of 10 degrees.

For the autotransformer at substations 3 and generator step-up (GSU) transformer at substation 2, SEAEs are shown in the left plot and right plot in Fig.4, respectively, as functions of the angle of the extra field. The transformer at substation 3 and transformer at substation 2 are located 51 km and 220 km away from the center of the localized field enhancement area, respectively. The significant magnitude difference shown in Fig.3

implies that the impact of the localized field enhancement on the transformers decreases rapidly as their distances from the localized field enhancement area increase. Also, the plots in Fig.3 appear to be in phase. However, this situation is not universal and only occurs due to the limited size of the system. There will be more discussions on this matter later.

Table 1
SEAE and EAEs for Two Transformers under an Eastward Extra Field

	Transformer at Sub 3	**Transformer at Sub 2**
SEAE	16.32	1.80
EAE From Line 15-6,1	8.16	0.90
EAE From Line 15-6,2	8.16	0.90
EAE From Line 21-11	0	0

Next, with the extra field fixed at 90 degrees (eastward), EAEs contributed by lines are recorded in Table 1 for the transformers at substation 3 and substation 2 in the second column and third column, respectively. As the lines making zero EAE contribution are omitted from Table 1, it is found that only three lines make contributions to EAEs. Line 21-11 is not omitted from Table II, because the values of EAEs contributed by line 21-11 are actually not zero (on the order of 10^{-6}) but rounded to zero. Since the magnitude of the extra field is 1 V/km, the EAE contributed by each line corresponds to a summation term in (17). Therefore, as shown in the second row of Table 1, the SEAE for each of the

transformers can be obtained by summing the EAEs contributed by the lines in the corresponding column.

With reference to Fig.3, line 15-6,1 and line 15-6,2 comprise the double-circuit line (in purple) between substation 3 and substation 6, while the line 21-11 comprises the single-circuit line (in yellow) between substation 5 and substation 7. It is observed that only the three lines passing through the localized field enhancement area make contributions to EAEs, considering that the extra field giving rise to EAEs only exists in the localized field enhancement area.

Another observation is that the EAEs contributed by line 15-6,1 and line15-6,2 are much higher than that contributed by line 21-11 (small enough to be grounded to zero) for both of the transformers. With reference to Fig.3, line 15-6,1 and line 15-6,2 are found to have much longer segments passing through the localized field enhancement area than line 21-11. This observation suggests that localized field enhancements tend to impact transformers through lines with longer segments falling inside the localized field enhancement than through lines with shorter segments. It is worth noting that the foregoing is just a tendency, since the values of EAEs also depend on the angle differences between the lines and extra field, based on (16).

Moreover, it is observed that the phase angles of the two plots in Fig.4 are both around 110 degrees. The observation can be explained by the fact that the phase angles of the plots in Fig.4 exclusively depend on the compass angles of line 15-6,1 and line 15-6,2, which are both 108.54 degrees. In other words, the appearance of the two plots in phase is

attributed to the little diversity of the lines passing through the localized field enhancement area and less likely to be observed in large cases.

B. 10k-bus Synthetic Network

In this section, sensitivity analysis is conducted on a 10k-bus synthetic network [14]-[16] in three stages. In stage one, five localized field enhancement areas with different locations and dimensions are applied to the system individually. The impact scope of each localized field enhancement is evaluated using the worst-case SEAE. In stage two, SEAEs for six selected transformers are determined, as the extra geoelectric field varies in direction. In stage three, effective GICs for two transformers are determined using (19) as the extra geoelectric field varies in magnitude.

The motivation for stage one is to investigate the relationship between the physical characteristics such as location and dimension of a localized field enhancement and its impact scope. For the sake of convenience, the worst-case SEAE is preferred over SEAE to avoid the SEAE's dependence on the angle differences between the lines and extra field. Therefore, the magnitude and direction of the extra field are not necessarily to be specified here. 0.1 A·km/V and 1 A·km/V are arbitrarily chosen as the thresholds with which the worst-case SEAE of each transformer is compared to determine whether the transformer is classified as impacted by the localized field enhancement. The impact scope of a localized field enhancement is quantified by the radius of the smallest circle that contains all the transformers with their worst-case SEAEs exceeding the threshold. The smallest circle is referred as the minimal circle in this work.

Table 2
Impact Scopes of Five Localized Field Enhancements

Local Enhancement Center	47º N, 120º W	39.5º N, 105º W	36º N, 116.5º W	40.5º N, 111º W	39.5º N, 119º W
Local Enhancement Width	300 km	400 km	500 km	500 km	600 km
Radius of the Minimal Circle (Threshold = 0.1 A·km/V)	726 km	565 km	678 km	735 km	718 km
Ratio of Radius to Width (Threshold = 0.1 A·km/V)	2.42	1.41	1.36	1.47	1.20
Radius of the Minimal Circle (Threshold = 1 A·km/V)	556 km	403 km	521 km	675 km	706 km
Ratio of Radius to Width (Threshold = 1 A·km/V)	1.85	1.00	1.04	1.35	1.18

Five square localized field enhancements, with their centers and widths shown in the first and second rows of Table 2, are applied to the 10k-bus synthetic network individually. The impact scopes for the five localized field enhancements are evaluated based on different impact evaluation criteria (0.1 and 1 A·km/V) and shown in the third and fifth rows, respectively. The ratio of the minimal circle's radius to the square localized field enhancement's width is used to illustrate the relationship between the impact scope and the dimension of the localized field enhancement and presented in the fourth and sixth rows of Table 2. The impact scopes of most of the examined localized field enhancements are observed to be similar in size to themselves. To be specific, the radii of their impact scopes are less than 1.5 times their own widths, even given a conservative evaluation criterion (0.1 A·km/V). However, an exception is also observed in this study that the smallest localized field enhancement (300 km by 300 km) has a comparatively large

impact scope with respect to its own size (1.85 times its width with 1 A·km/V criterion and 2.42 times its width with 0.1 A·km/V criterion). It is found that multiple high-voltage (765 kV) long-distance transmission lines emanating from the localized field enhancement area bring its impact farther through the power grid. To avoid electric field concentration, long-distance high-voltage transmission lines are designed with lower resistances and subject to higher GICs [2], [21]. Therefore, the worst-case SEAEs for the transformers with close electrical connections to these lines are high.

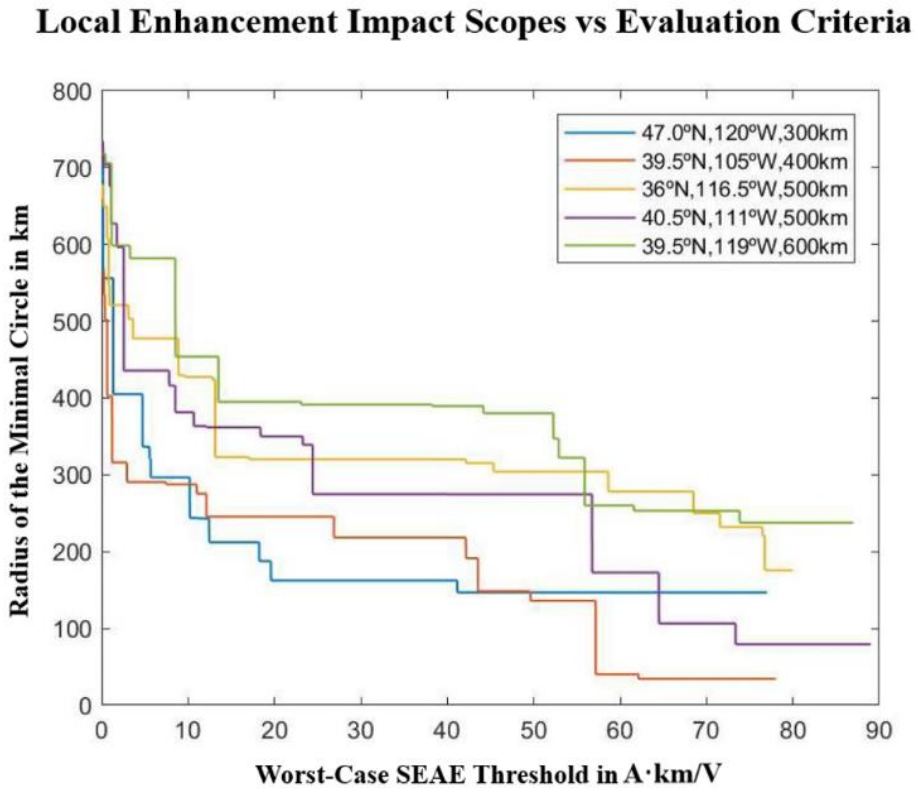

Fig.5. The impact scopes of the five selected localized field enhancements versus different evaluation criteria (thresholds) with which the worst-case SEAEs of transformers are compared to determine whether the transformers are under impact.

Considering the variation in the impact scopes based on different thresholds, Fig.5 provides an approximate mapping between the impact scopes and impact evaluation criteria for the five localized field enhancements.

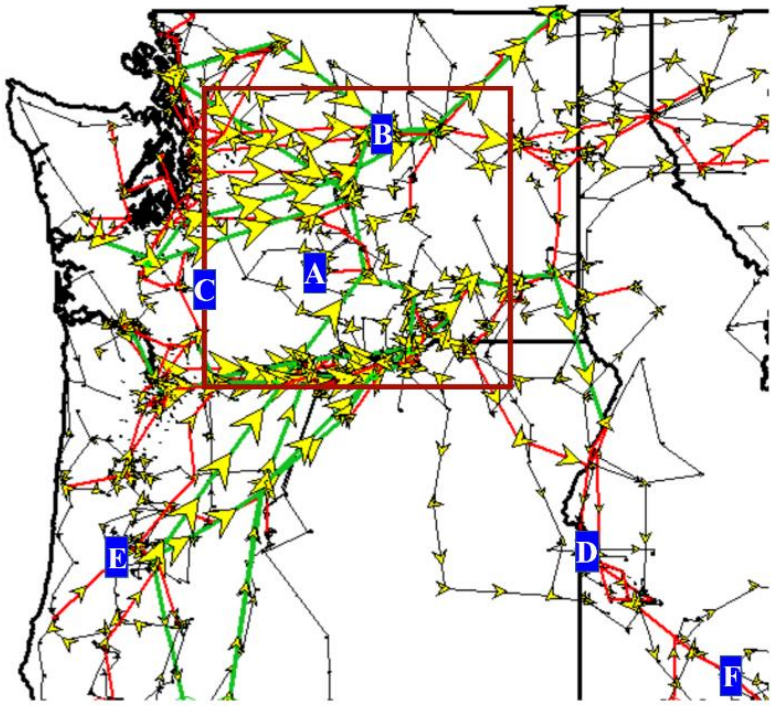

Fig.6. The portion of the 10k-bus system that includes the power grids in Washington, Oregon, Idaho, and Montana. The system is synthetic and does not represent the actual grids in these states. The boundary of the 300 km by 300 km local enhancement area is indicated by the red square. The geoelectric fields inside and outside the area are 2 V/km and 1 V/km, respectively, and both of 90 degrees. The yellow arrows represent GICs and A-F fields show the locations of the selected transformers.

In stage two, six transformers are selected to undertake the same sensitivity analysis performed on the 20-bus system from the previous section. The same GMD scenario is taken here, but with the center and width of the square localized field

enhancement changed to (47º N, 120º W) and 300 km. Fig.6 shows the portion of the 10k-bus system that includes the power grids in Washington, Oregon, Idaho, and Montana. The boundary of the localized field enhancement area is marked by the red square and the locations of the six selected transformers are indicated as the A-F text fields. Transformer A, D, E are 345/138 kV autotransformers, while transformer B, C, and F are 765/22 kV GSU, 138/13/13 kV three-winding transformer, and 345/14 kV GSU, respectively. The yellow arrows in Fig.6 show the magnitudes and directions of the GICs, where the system is subjected to a 90-degree base field and extra field.

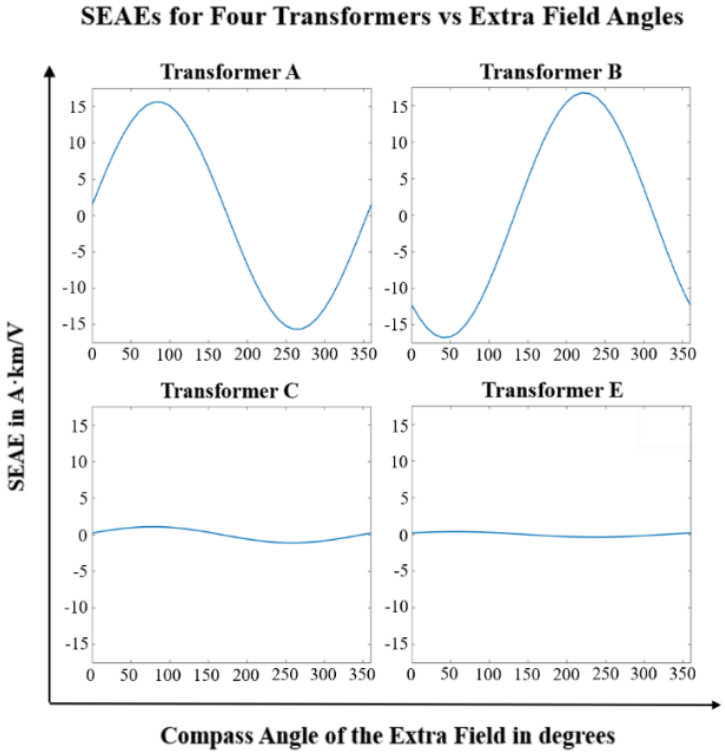

Fig.7. The variation in SEAE for the transformer A, B, C, and E with the compass angle of the extra field varying from 0 to 360 degrees in steps of 10 degrees.

Considering that GICs flow in the same direction as the yellow arrows and have magnitudes proportional to the size of the yellow arrows, the high-voltage transmission lines (765kV lines are in green and 345kV lines are in red in Fig.6.) are subjected to high GICs.

SEAE is determined for each of the six selected transformers as the extra field varies in direction from 0 to 360 degrees in increments of 10 degrees. The SEAEs for transformers D and F are found to be negligible and not explicitly presented here, while the SEAEs for the rest of the transformers are presented in Fig.7. The plots in Fig.7 are observed to be out of phase with each other, which contradicts the seemingly in-phase plots shown in the previous section. Since the phase angle of such a plot depends on the characteristics of both the network and localized field enhancement, the plots associated with different transformers most likely have different phase angles.

Another observation from Fig.7 is that the plots for the transformers inside the localized field enhancement area have much higher magnitudes than those for the ones outside the area. This indicates that the impact of a localized field enhancement area doesn’t propagate far outside the area. In this specific case, transformer F, located about 600km away from the center of the localized field enhancement area, is not impacted anymore. This result is consistent with the observation made in stage one where worst-case SEAEs were used to measure the impact. However, it is worth noting that the plot for transformer C, outside but near the boundary, has a similar magnitude as that for transformers E, far from the boundary. This observation indicates that a transformer’s proximity to a localized field enhancement does not guarantee a large impact from the

localized field enhancement, since various factors such as the transformer's voltage level, transmission lines' orientations, and localized field enhancement's physical characteristics all affect the degree of impact. Yet, at first glance, the distance between a transformer and a localized field enhancement gives a reasonable approximation of the likelihood of the transformer being impacted.

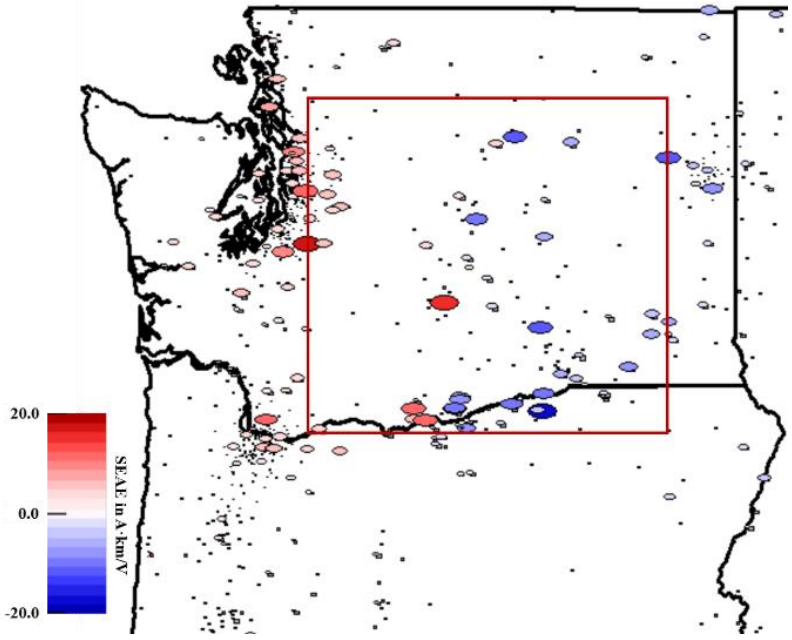

Fig.8. The extra field is fixed at 90 degrees (eastward). The red square indicates the boundary of the (300 km by 300 km) localized field enhancement, while the ovals represent transformers. The sizes of the ovals are proportional to the magnitudes of the transformers' SEAEs, while the fill colors illustrate the actual values of the SEAEs.

To show the distribution of the impacted transformers, with the extra field fixed at 90 degrees, the SEAEs for the transformers are visualized in Fig.8 using geographic data views [22]. At each substation, one transformer is selected to represent all its transformers.

Each representative transformer has the largest SEAE magnitude among the set of transformers with the highest voltage levels. Each oval indicates a representative transformer where the size of the oval is proportional to the absolute value of the SEAE and the fill color of the oval shows the actual value of the SEAE. To keep consistent with the impact evaluation criterion used in stage one, the ovals for the representative transformers with their SEAE magnitudes lower than 1 A·km/V are omitted from Fig.8. Considering that the red square shows the boundary of the localized field enhancement area, it is observed that most of the transformers outside the area are not subjected to the impact of the localized field enhancement just with a few exceptions west of the boundary.

During the previous two stages, the impact of a localized field enhancement was examined from the sensitivities' point of view. In stage three, based on (19), the effective GICs for transformers A and C are determined under an extra field with a varying magnitude. The 300 km by 300 km localized field enhancement centered at (47º N, 120º W) is considered here again.

Table 3
Effective GICs for Transformer A as Extra Field Varies in Magnitude

E_u (V/km)	E_c (V/km)	$I_{AEff,u}$ (A)	ΔI_{AEff} (A)	I_{Eff} (A)
1	1	14.410	15.600	30.010
1	2	14.410	31.200	45.610
1	3	14.410	46.800	61.210

Table 4
Effective GICs for Transformer C as Extra Field Varies in Magnitude

E_u (V/km)	E_c (V/km)	$I_{AEff,u}$ (A)	ΔI_{AEff} (A)	I_{Eff} (A)
1	1	-11.951	1.076	10.874
1	2	-11.951	2.153	9.798
1	3	-11.951	3.229	8.721

Except the localized field enhancement area, the 10k-bus network is subjected to a 90-degree base geoelectric field of 1 V/km. Meanwhile, the localized field enhancement area is subjected to a 90-degree geoelectric field where its magnitude increases from 2 to 4 V/km in steps of 1 V/km. Table 3 and Table 4 show the base field magnitudes (E_u), extra field magnitudes (E_c), the actual effective GICs ($I_{AEff,u}$) due to the base field, the extra actual effective GICs (ΔI_{AEff} or EAE) due to the extra field, and the effective GICs (I_{Eff}) for transformer A and transformer C, respectively. According to Table 3 and Table 4, the SEAEs for transformer A and transformer C are 15.6 and 1.076 A·km/V. For both of the transformers, ΔI_{AEff} (EAE) is observed to vary linearly with the extra field magnitude, whereas I_{Eff} is observed to vary nonlinearly. It is also observed that the I_{Eff} of transformer A is positively correlated with the extra field's magnitude, whereas the I_{Eff} of transformer C is negatively correlated.

In fact, such a negative correlation is observed in many transformers near the boundary of the localized field enhancement area and with their nearby lines (The nearby lines of a transformer are defined as the lines connecting the transformer to the neighbor buses.) passing through the area. For each of these boundary transformers, the ΔI_{AEff}

contributed by the line segments falling inside the localized field enhancement area has the opposite sign of the $I_{AEff,u}$ contributed by all the lines. In other words, if the GICs induced by the extra field flow in the opposite direction as the GICs induced by the base field, a negative correlation between the transformer's I_{Eff} and extra field's magnitude can be observed.

CHAPTER III [1]

IMPACT OF GEOMAGNETIC DISTURBANCES ON POWER SYSTEM TRANSIENT STABILITY

Background

A. Motivation for Research

In contrast to the impacts of GMDs on systems' static characteristics (i.e. steady-state operating conditions), the impacts of GMDs on systems' dynamic characteristics (i.e. transient) have been seldomly studied or considered in reliability criteria. To promote research on system dynamic response under the effect of GMDs, it is crucial to show that GMDs can alter power system transient stability margin.

B. Literature Review and Research Approach Overview

Using the same 10k-bus synthetic network [14]-[16] from Chapter 1, this work examines the impacts of GMDs on the power system transient stability following different single element contingencies. Previous works such as [23] and [24] investigated the transient voltage stability of small systems under the effect of GMDs. Reference [23] examined how the ramping rates of electric fields, load models, and voltage controls influence the voltage stability. Reference [24] studied how different characteristics of electric fields impact the transient voltage stability during a high-altitude electromagnetic

[1] © [2018] IEEE. Reprinted, with permission, from [Yiqiu Zhang, Impact of Geomagnetic Disturbances on Power System Transient Stability, 2018 North American Power Symposium (NAPS), Sept. 2018]

pulse (HEMP), a special GMD event as a result of a nuclear explosion. Both of the papers used GMDs as the disturbances to the systems, with the severity levels of the disturbances dependent on the characteristics of the electric fields such as rise time, decay time, and duration. Instead, this study uses the typical single element contingencies as the disturbances and assumes a constant electric field throughout each simulation. The assumption of a constant electric field is justified by the fact that naturally-occurring GMDs, usually with frequencies much below 1 Hz, do not vary much during the transient time frame of several dozen seconds. Moreover, the variations in voltage stability and rotor angle stability [25] of the 10k-bus system are evaluated using different metrics (e.g. maximum voltage drop and critical clearing time).

C. GIC Modeling in Transient Stability

This section gives an overview of how GICs are modeled in transient stability analysis in [24]. GICs induced in transmission lines impact power systems by causing half-cycle saturation of transformers and in turn increasing the reactive power losses in the transformers. For each of the transformers, the reactive power loss due to GICs can be determined by solving

$$Q_{Loss,pu} = V_{pu} K I_{GIC,pu} \tag{1}$$

where $Q_{Loss,pu}$ is the reactive power loss; V_{pu} is the ac voltage of the transformer's high-side terminal bus; K is a constant which maps the GICs to the losses and depends on the

characteristics of the transformer; $I_{GIC,pu}$ is an adjusted version of the GIC where the transformer parameters are incorporated [26], [17], [18]. All the variables with the subscript "pu" are expressed in per unit. GICs participate in the dynamics of the system as additional constant current reactive loads and alter the reactive power balance equations of the transient stability model [24] as follows.

$$Q_{Gen,i} - Q_{L,i} - Q_{Loss,i} - \sum_{k=1}^{n} V_i V_k Y_{ik} \sin(\theta_i - \theta_k - \alpha_{ik}) = 0, \quad i = 1, \ldots, m \tag{2}$$

$$- Q_{L,i} - Q_{Loss,i} - \sum_{k=1}^{n} V_i V_k Y_{ik} \sin(\theta_i - \theta_k - \alpha_{ik}) = 0, \quad i = m+1, \ldots, n \tag{3}$$

Equation (2) and equation (3) show the reactive power balance at a generator bus and a load bus, respectively. The system has n buses in total, m among which are the generator buses. The reactive power consumed by loads at bus i is represented as $Q_{L,i}$. At a high-side terminal bus i of a transformer, the reactive power loss due to GICs is represented as $Q_{Loss,i}$. At a generator bus i, the reactive power supplied by generators is represented by $Q_{Gen,i}$. V and θ are the bus voltage and bus angle with the subscript (i, k) showing the bus number. The admittance between bus i and bus k and associated angle are given by Y_{ik} and α_{ik}, respectively [24]. With combination of a set of differential equations and other constraints [27], the system states can be determined using numerical integration. Equation (1) will be performed at each iteration to update $Q_{Loss,i}$ in (2) and (3).

GMD Transient Stability Case Studies

A. Voltage Transient Stability Analysis for a Generator Outage

In the presence of a time-invariant and uniform electric field, the voltage transient stability of the 10k-bus system is examined following the loss of one of the biggest generators in Arizona. The electric field has a direction of 77 degrees, with north as the reference (0 degrees). A 77-degree electric field is chosen, because it will result in the maximum reactive power loss for the system. The electric field is increased from 0 to 7 V/km (The power flow does not converge beyond 7 V/km.) in steps of 1V/km. 0 V/km electric field is equivalent to "in the absence of a GMD". Under the electric field, the generator is opened at the first second and the next nineteen seconds of voltage response is recorded for a bus in Arizona and a bus in Oregon, respectively. These buses are selected for their relatively large variations in their maximum voltage drops in the presence of GMDs.

The opened generator in Arizona is connected to a high voltage bus (765 kV) though a generator step-up (GSU) transformer. Under normal conditions (i.e. in the absence of a GMD), the generator provides 1397.5 MW, and is at its maximum Mvar output limit of 516.4 Mvar, with its maximum MW output limit to be 1403.2 MW.

The impact of the GMDs on the voltage transient stability of a bus in Arizona is evaluated. The bus of interest is the high-side terminal bus of a 500kV-115kV transformer.

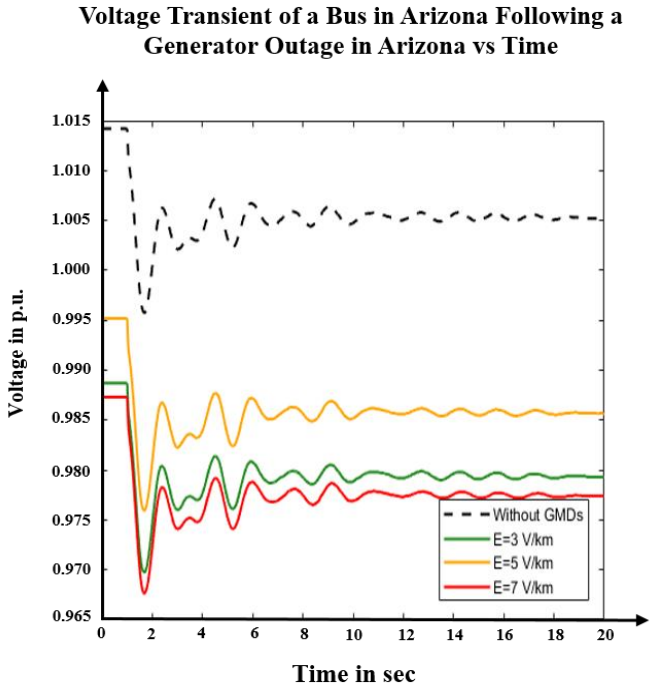

Fig.9. The actual pre-contingency voltage values and transient voltage response of a bus in Arizona after the occurrence of the generator outage in Arizona under the effect of different GMDs. Reprinted with permission from [Yiqiu Zhang, Impact of Geomagnetic Disturbances on Power System Transient Stability, 2018 North American Power Symposium (NAPS), Sept. 2018]

Fig.9 shows the actual initial voltage values in the first second (before the occurrence of the contingency) and voltage transients for the next nineteen seconds of the bus. The curves in different colors represent the voltages of the same bus, with the system subjected to the 77-degree electric fields with different magnitudes (i.e. 0, 3, 5, and 7 V/km), respectively. Since power flow solutions determine the initial voltages prior to the contingency and the electric field magnitudes determine the reactive power losses due to GICs, the initial voltage of the bus in Arizona is observed to vary with different electric field magnitudes. However, the initial voltage is not positively correlated to the electric field magnitude, given that the yellow curve (E = 5 V/km) is above the green curve (E =

3 V/km) in Fig.9. This observation is caused by the inclusion of shunt switching in the power flow. In the presence of the 5 V/km electric field, discrete capacitor switching near the bus in Arizona is observed, which explains why the initial voltage under this condition is greater than that under a lower electric field level.

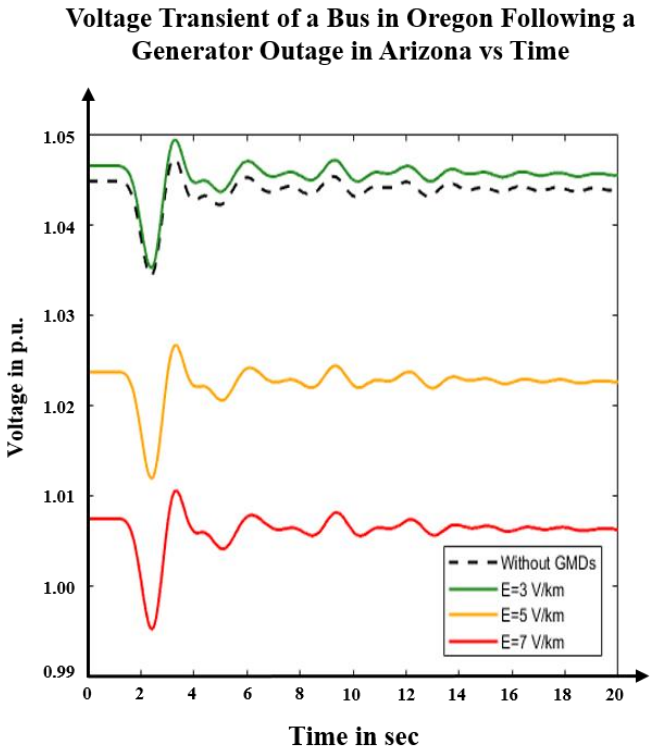

Fig.10. The actual pre-contingency voltage values and transient voltage response of a bus in Oregon after the occurrence of the generator outage in Arizona under the effect of different GMDs. Reprinted with permission from [Yiqiu Zhang, Impact of Geomagnetic Disturbances on Power System Transient Stability, 2018 North American Power Symposium (NAPS), Sept. 2018]

Following the generator outage, the transient voltage response of a bus in Oregon is also recorded and shown in Fig.10, which is organized the same way as Fig.9. The bus of interest is the high-side terminal bus of a 765kV-345kV transformer and connected to four small generators, through GSU transformers. The same set of observations made from

Fig.9 can also be made from Fig.10. Under the effect of GMDs, changes in voltage dynamics, reflected by changes in the maximum voltage drop, are also observed and shown in Table 5 and Table 6 for the bus in Arizona and the bus in Oregon, respectively.

Table 5
Bus (Arizona) Voltage Summary under Electric Fields with Various Magnitudes
Reprinted with permission from [Yiqiu Zhang, Impact of Geomagnetic Disturbances on Power System Transient Stability, 2018 North American Power Symposium (NAPS), Sept. 2018]

Electric Field Magnitude (V/km)	Initial Voltage (p.u.)	Maximum Voltage Drop (p.u.)	Lowest Voltage (p.u.)
0	1.0142	0.0185	0.9957
3	0.9887	0.019	0.9697
5	0.9952	0.0193	0.9759
7	0.9873	0.0197	0.9676

Table 6
Bus (Oregon) Voltage Summary under Electric Fields with Various Magnitudes
Reprinted with permission from [Yiqiu Zhang, Impact of Geomagnetic Disturbances on Power System Transient Stability, 2018 North American Power Symposium (NAPS), Sept. 2018]

Electric Field Magnitude (V/km)	Initial Voltage (p.u.)	Maximum Voltage Drop (p.u.)	Lowest Voltage (p.u.)
0	1.0448	0.0108	1.0340
3	1.0465	0.0115	1.0350
5	1.0237	0.0117	1.0120
7	1.0075	0.0122	0.9953

Table 5 and Table 6 show the actual initial voltages, maximum voltage drops, and actual lowest voltages for the bus in Arizona and the bus in Oregon under the effect of the different electric fields, respectively. It is observed that the variation in initial voltage of either bus is on the order of 0.01 p.u., while the variation in maximum voltage drop for

either bus is on the order of 0.001 p.u. Therefore, the variations in lowest voltages are more dependent on the changes in initial voltages than on the changes in system dynamics. Moreover, there is a positive correlation between the maximum voltage drop and electric field magnitude observed in Table 5 and Table 6, which suggests that GICs may tend to negatively impact the voltage transient stability of the system. Given the monitored buses' distances from the contingency, GICs can not only impact the voltage transient of the buses near the contingency, but also those of the buses far from the contingency.

B. Rotor Angle Transient Stability Analysis for a Transformer Outage

In this section, the rotor angle transient stability of the system is examined following the loss of an EHV transformer in Arizona. The rotor angle transient of a generator in Arizona is monitored in the absence of a GMD or in the presence of a 77-degree uniform electric field (with north as 0 degrees) of 1 V/km or of 2 V/km. Since the generator experiences an unacceptable increment and instability in its rotor angle under the 1 V/km electric field and under the 2 V/km electric field, respectively, the usage of a metric becomes unnecessary in this case.

A 500kV-115kV autotransformer with both its windings grounded is opened at the first second in Arizona. Under the electric field of 1 V/km, the reactive power absorbed by the transformer is 35.36 Mvar. With the magnitude of the electric field increasing to 2 V/km, the reactive power absorption increases to 70.71 Mvar. Since the reactive power loss imposed on the transformer due to GICs is modeled as a constant current reactive load, the system will experience a sudden reactive load loss upon the transformer outage.

The generator of interest is located at a substation, named NOGALES, in Arizona and connected to the high-side terminal bus of a 500kV-115kV wye-wye grounded autotransformer through a GSU transformer. The generator can provide a maximum of 27 MW and 13.743 Mvar. The substation containing the opened transformer is connected to substation NOGALES by a 500kV 77km long transmission line. The machine, exciter, governor, and stabilizer models of the monitored generator are GENROU, EXPIC1, GGOV1, and IEEEST, respectively [28].

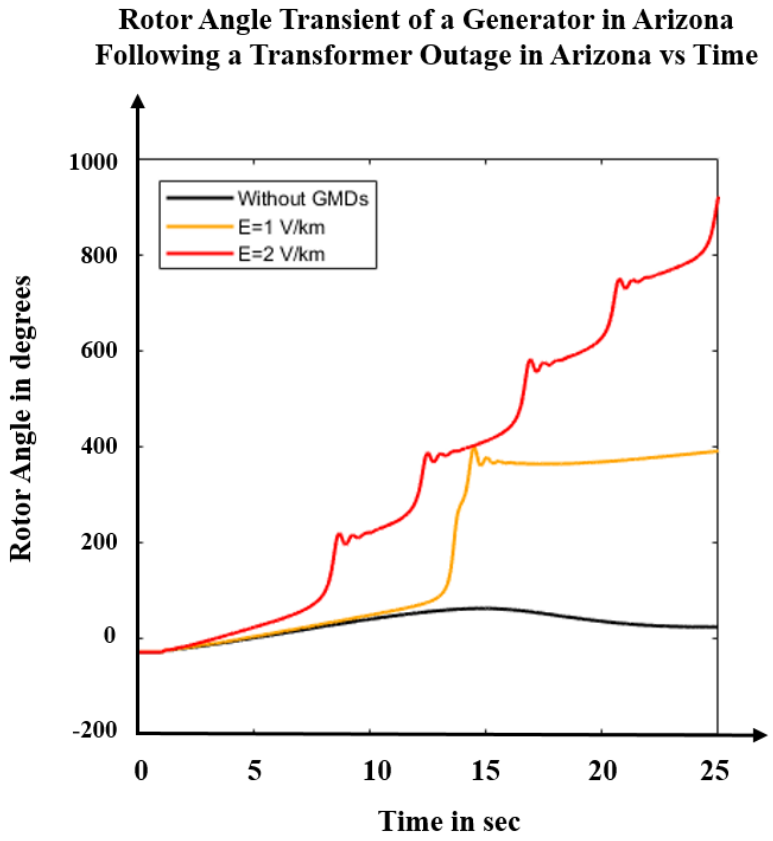

Fig.11. An EHV transformer in Arizona is opened at t = 1 sec. The rotor angle of a generator at a substation, named NOGALES, in Arizona is monitored in the absence or presence of GMDs. Reprinted with permission from [Yiqiu Zhang, Impact of Geomagnetic Disturbances on Power System Transient Stability, 2018 North American Power Symposium (NAPS), Sept. 2018]

The rotor angle of the monitored generator in Arizona in the absence or presence of a GMD is presented in Fig.11. Fig.11 shows the pre-contingency rotor angle in the first second and the rotor angle transient for the next twenty four seconds following the transformer outage. In the absence of a GMD, the rotor angle increases from -27 to 63.7 degrees and eventually reaches an equilibrium rotor angle of 37.6 degrees. In the presence of the 77-degree electric field of 1 V/km, the rotor angle of the generator experiences a 425.7-degree increment, settling at 405.9 degrees.

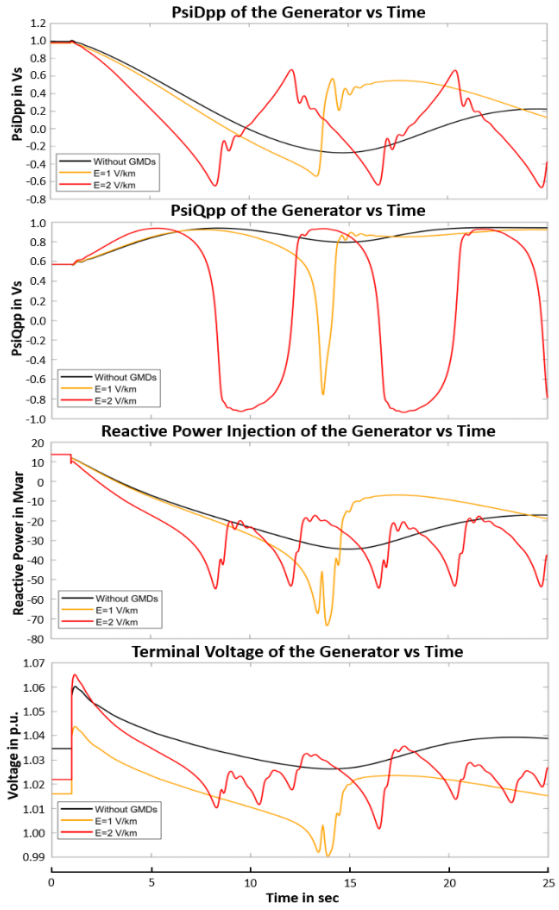

Fig.12. State variable variations for the monitored generator in the absence of a GMD or in the presence of different GMDs. Reprinted with permission from [Yiqiu Zhang, Impact of Geomagnetic Disturbances on Power System Transient Stability, 2018 North American Power Symposium (NAPS), Sept. 2018]

However, such a significant change in a generator rotor angle is prohibited in actual power system operations, since the change can cause an unacceptable power swing and make the system less secure. Practically, a generator experiencing a significant change in its rotor angle will be disconnected from the system by out-of-step protective relays to prevent equipment damage, and other system effects. The red curve in Fig.11 indicates that the rotor angle of the generator becomes unstable under the effect of the 77-degree electric field of 2 V/km.

Fig.12 provides the variations in different state variables of the monitored generator. The first two subplots show flux linkage variations (i.e. PsiDpp and PsiQpp) of the generator, while the third and fourth subplots show the Mvar injection and terminal voltage magnitude, respectively. The black, yellow, and red lines in each subplot show the variations in the corresponding state variable at E = 0 V/km (in the absence of a GMD), E = 1 V/km, and E = 2 V/km, respectively. Upon the transformer outage (at t = 1 sec), the terminal voltage of the generator spikes as the result of a sudden increase in Mvar flow into substation NOGALES. The generator reduces its Mvar injection into the network and even starts to absorb Mvar out of the network, as the Mvar flow into substation NOGALES gradually increases. The above description and explanation apply to all three GMD scenarios considered here. At E = 1 V/km, the rate of change of the Mvar flowing into substation NOGALES starts to increase around t = 12 sec until the valve opening/closing rate limit of the generator's governor is violated around t = 13.5 sec. This violation may trigger a control action which causes the reactive power injection to change from decreasing to increasing and stabilizes the generator's rotor angle around t = 13.5 sec, as

shown in Fig.11. At E = 2 V/km, the same limit violation occurs around t = 8.3 sec. The same reasoning can also be used to explain why the red line in the third subplot changes from decreasing to increasing at that time. This case suggests that GMDs can potentially cause rotor angle instability through a relatively low electric field. During a severe GMD event, GICs will substantially increase and saturate transformers, especially EHV and UHV transformers. The transformers can be permanently damaged from overheating. The outage of the transformers in such an event will result in more serious consequences, given that the system is burdened with a high reactive power demand and faced with a large disturbance caused by the sudden loss of a significant amount of reactive load.

Average Bus Frequency Responses at Substations in the Presence of Different Electric Fields

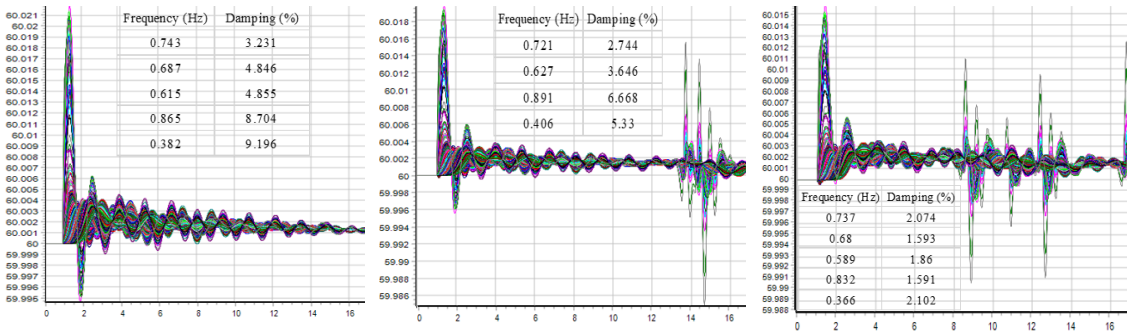

(a) E=0 V/km **(b) E=1 V/km** **(c) E=2 V/km**

Fig.13. An EHV transformer in Arizona is opened at t =1 sec. The average of bus frequencies at each substation is shown for different electric fields. Reprinted with permission from [Yiqiu Zhang, Impact of Geomagnetic Disturbances on Power System Transient Stability, 2018 North American Power Symposium (NAPS), Sept. 2018]

Fig.11 shows the rotor angle of a single generator under different GMD conditions. We now look at bus frequency responses of the same set of simulations, such as those that

may be recorded by devices such as PMUs, to assess the system wide effects. The average of bus frequencies at each substation is the selected signal in this analysis.

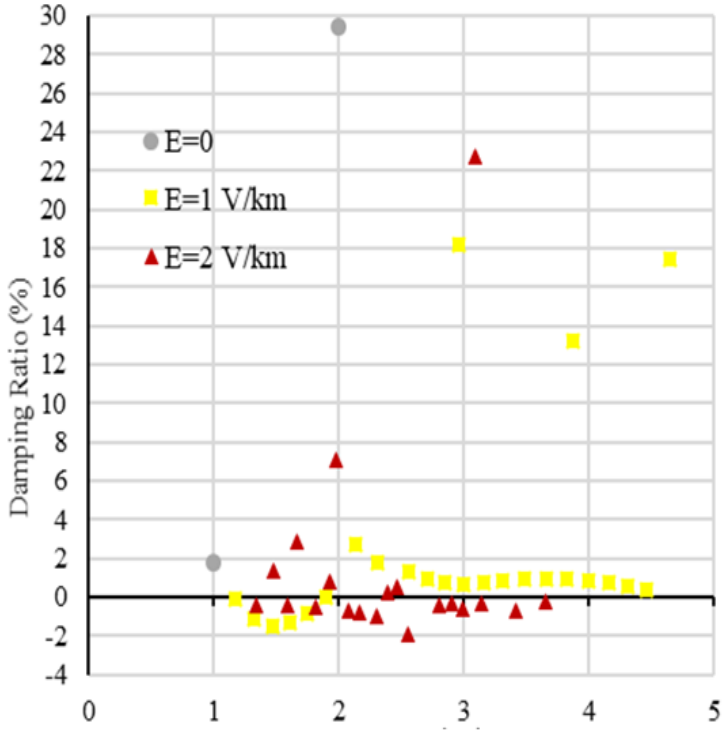

Fig.14. Modes of oscillation versus their damping ratios where the largest weighted percentage signal is from substation NOGALES. Reprinted with permission from [Yiqiu Zhang, Impact of Geomagnetic Disturbances on Power System Transient Stability, 2018 North American Power Symposium (NAPS), Sept. 2018]

In the absence of a GMD, both Fig.11 and Fig.13 (a) indicate that the system is stable. Fig.13 (b) shows the sudden commencement of oscillations observed at several buses at around t = 13 sec, which coincides with the onset of the rotor angle instability in Fig.11. Similarly, Fig.13 (c) shows oscillations earlier, at around t = 9 sec. There is a certain periodicity in these results (i.e. t = 9, 13, 17 and so), which match up with the times when the “notches” occur in the red curve in Fig.11. Fig.14 also shows the key modes

with low damping ratios (i.e. < 10%) for each scenario. The damping of these modes reduces progressively as the applied electric field increases. Moreover, the electric field introduces instabilities, by causing negatively damped oscillations most from one particular generating substation named NOGALES. These are shown in Fig.14.

C. Rotor Angle Transient Stability Analysis for a Temporary Balanced Three-Phase Line Fault

In this section, the rotor angle transient stability of the system is examined following a balanced three-phase fault on a line in Utah. The critical clearing time (CCT) of the fault is determined by observing the first occurrence of rotor angle instability under the effect of an electric field at 77 degrees, with north as the reference. The magnitude of the electric field varies from 0 to 4 V/km in steps of 1 V/km. 0 V/km electric field is equivalent to "in the absence of a GMD".

CCT is a commonly used metric for evaluating the transient stability of a system in a short circuit analysis [29]. CCT is defined as the maximum duration for which a short-circuit fault can last without the system losing its synchronism [29]. This section determines the CCT by gradually increasing the fault duration in the steps of 0.001s and using the time just before the observation of the first unstable rotor angle of a generator.

A balanced three-phase fault is applied to a 56.8 km long 500kV transmission line in Utah. The substations connected by the line have no generators. With no GMD or 77-degree electric fields of varying magnitudes applied to the 10k-bus system individually, the critical clearing time of the fault is determined.

Table 7
CCTs under Electric Fields with Various Magnitudes

Reprinted with permission from [Yiqiu Zhang, Impact of Geomagnetic Disturbances on Power System Transient Stability, 2018 North American Power Symposium (NAPS), Sept. 2018]

Electric Field Magnitude (V/km)	Critical Clearing Time (s)
0	0.427
1	0.421
2	0.419
3	0.411
4	0.404

Table 7 shows that CCT decreases as the electric field magnitude increases. Moreover, it is observed that the rotor angle of the generator nearest to the faulted line always becomes unstable first regardless of the magnitude of the applied electric field. This observation can be explained by the fact that generators, especially the ones close to the contingency, are more stressed due to increased reactive power demand under the effect of increased GICs. In this specific case, the CCTs in the presence of GMDs are shorter than that in the absence of a GMD. As a result of a decreased CCT, the circuit breakers designed for normal conditions (in the absence of a GMD) may not be able to react promptly in the presence of GMDs. Equipment damage and service interruption are more likely to occur in this situation.

CHAPTER IV

SUMMARY AND CONCLUSION

The work specified in Chapter II investigated the impact scopes of localized field enhancements by using the superposition principle and defining sensitivities, SEAEs, associated with the "extra" fields. The results from sensitivity analysis, conducted respectively on a 20-bus system and on a 10k-bus system, suggest that the impact scope of a square localized field enhancement area is generally less than 1.5 times its width. An exception may occur when high-voltage long-distance transmission lines emanate from the localized field enhancement area and propagate the impact farther out (The studied example showed that the impact scope of such a square localized field enhancement area might reach 2.5 times its width.). It is also found that localized field enhancements tend to impact transformers more through the lines with longer segments falling inside the localized field enhancement areas than through the lines with shorter segments. For some transformers near the boundary of a localized field enhancement, their effective GICs are observed to vary negatively with the magnitude of the "extra" field, as the GICs induced by the extra field flow in the opposite direction as the GICs induced by the base field.

The work specified in Chapter III investigated the impacts of GMDs on power system transient stability following different single element contingencies, by performing case studies on the 10k-bus synthetic network. Both of the voltage stability and rotor angle stability were evaluated using the maximum voltage drop and critical clearing time as the metrics, respectively. The results of the case studies suggest that power system transient

margin can be altered by the presence of GMDs. After the occurrence of a generator outage, the maximum voltage drop of a bus near the generator and a bus far from the generator was observed to vary positively with the electric field magnitude. Moreover, GICs due to a relatively low electric field were observed to be detrimental to the rotor angle transient stability and synchronism of certain generators following the loss of an element such as a transformer. Also, the change in rotor angle dynamics evaluated using the critical clearing time of a balanced three-phase fault was observed under the effect of GMDs. The key takeaway from the research is that in addition to steady state power flow studies, transient stability studies may also need to be conducted to adequately plan and prepare for operating grids securely in the presence of GMDs.

REFERENCES

[1] “March 13, 1989 Geomagnetic Disturbance,” NERC. Available: https://www.nerc.com/files/1989-Quebec-Disturbance.pdf

[2] V. D. Albertson, J. M. Thorson, R. E. Clayton and S. C. Tripathy, "Solar-Induced-Currents in Power Systems: Cause and Effects," in *IEEE Transactions on Power Apparatus and Systems*, vol. PAS-92, no. 2, pp. 471-477, March 1973.

[3] W. A. Radasky, "Overview of the impact of intense geomagnetic storms on the U.S. high voltage power grid," *2011 IEEE International Symposium on Electromagnetic Compatibility*, Long Beach, CA, USA, 2011, pp. 300-305.

[4] V. D. Albertson, J. M. Thorson and S. A. Miske, "The Effects of Geomagnetic Storms on Electrical Power Systems," in *IEEE Transactions on Power Apparatus and Systems*, vol. PAS-93, no. 4, pp. 1031-1044, July 1974.

[5] D. H. Boteler and E. Bradley, "On the Interaction of Power Transformers and Geomagnetically Induced Currents," in *IEEE Transactions on Power Delivery*, vol. 31, no. 5, pp. 2188-2195, Oct. 2016.

[6] J. G. Kappernman and V. D. Albertson, "Bracing for the geomagnetic storms," in *IEEE Spectrum*, vol. 27, no. 3, pp. 27-33, March 1990.

[7] "Benchmark Geomagnetic Disturbance Event Description, " Project 2013-03 GMD Mitigation, NERC, Dec. 2014. [Online]. Available: http://www.nerc.com/pa/Stand/Project201303GeomagneticDisturbanceMitigation/Benchmark-GMD-Event-Dec5-redline.pdf

[8] "Supplemental Geomagnetic Disturbance Event Description, " Project 2013-03 GMD Mitigation, NERC, June. 2017. [Online]. Available: http://www.nerc.com/pa/Stand/Project201303GeomagneticDisturbanceMitigation/Supplemental_GMD_Event_Description_June_2017.pdf.

[9] T. J. Overbye, K. S. Shetye, T. R. Hutchins, Q. Qiu and J. D. Weber, "Power Grid Sensitivity Analysis of Geomagnetically Induced Currents," in *IEEE Transactions on Power Systems*, vol. 28, no. 4, pp. 4821-4828, Nov. 2013.

[10] R. J. Pirjola, "On the flow of geomagnetically induced currents in an electric power transmission network," Canadian J. Phys., vol. 88, no. 5, pp. 357–363, May 2010.

[11] D. H. Boteler, "The use of linear superposition in modelling geomagnetically induced currents," *2013 IEEE Power & Energy Society General Meeting*, Vancouver, BC, 2013, pp. 1-5.

[12] D. H. Boteler, Q. Bui-Van and J. Lemay, "Directional sensitivity to geomagnetically induced currents of the Hydro-Quebec 735 kV power system," in IEEE Transactions on Power Delivery, vol. 9, no. 4, pp. 1963-1971, Oct 1994.

[13] R. Horton, D. Boteler, T. J. Overbye, R. Pirjola and R. C. Dugan, "A Test Case for the Calculation of Geomagnetically Induced Currents," in IEEE Transactions on Power Delivery, vol. 27, no. 4, pp. 2368-2373, Oct. 2012.

[14] A. B. Birchfield, T. Xu, K. M. Gegner, K. S. Shetye and T. J. Overbye, "Grid Structural Characteristics as Validation Criteria for Synthetic Networks," in IEEE Transactions on Power Systems, vol. 32, no. 4, pp. 3258-3265, July 2017.

[15] T. Xu, A. B. Birchfield, K. S. Shetye and T. J. Overbye, "Creation of synthetic electric grid models for transient stability studies," 2017 IREP Symposium Bulk Power System Dynamics and Control, Espinho, Portugal, 2017, pp. 1-6.

[16] Electric Grid Test Case Repository (2017). [Online]. Available: https://electricgrids.engr.tamu.edu/electric-grid-test-cases/activsg10k/.

[17] T. J. Overbye, T. R. Hutchins, K. Shetye, J. Weber and S. Dahman, "Integration of geomagnetic disturbance modeling into the power flow: A methodology for large-scale system studies," 2012 North American Power Symposium (NAPS), Champaign, IL, 2012, pp. 1-7.

[18] Hao Zhu and T. Overbye, "Blocking device placement for mitigating the effects of geomagnetically induced currents," 2016 IEEE Power and Energy Society General Meeting (PESGM), Boston, MA, 2016, pp. 1-1.

[19] D. H. Boteler and R. J. Pirjola, "Modelling geomagnetically induced currents produced by realistic and uniform electric fields," in IEEE Transactions on Power Delivery, vol. 13, no. 4, pp. 1303-1308, Oct 1998.

[20] V. D. Albertson, J. G. Kappenman, N. Mohan and G. A. Skarbakka, "Load-Flow Studies in the Presence of Geomagnetically-Induced Currents," in IEEE Transactions on Power Apparatus and Systems, vol.

[21] W. A. Radasky and J. G. Kappenman, "Impacts of geomagnetic storms on EHV and UHV power grids," 2010 Asia-Pacific International Symposium on Electromagnetic Compatibility, Beijing, 2010, pp. 695698.

[22] T.J. Overbye, E.M. Rantanen, S. Judd, "Electric power control center visualizations using geographic data views," Bulk Power System Dynamics and Control -- VII. Revitalizing Operational Reliability -- 2007 IREP Symposium, Charleston, SC, August 2007, pp1-8.

[23] T. J. Overbye, K. S. Shetye, Y. Z. Hughes and J. D. Weber, "Preliminary consideration of voltage stability impacts of geomagnetically induced currents," 2013 IEEE Power & Energy Society General Meeting, Vancouver, BC, 2013, pp. 1-5.

[24] T. R. Hutchins and T. J. Overbye, “Power system dynamic performance during the late-time (E3) high-altitude electromagnetic pulse,” in Power Systems Computation Conference (PSCC), 2016. IEEE, 2016, pp. 1-6.

[25] IEEE/CIGRE joint task force on stability terms and definition," definations and classifications of power system stability," IEEE Trans. Power Systems, vol. 19, no. 2.pp. 1387-1401, 2004.

[26] K. Zheng, "Effects of system characteristics on geomagnetically induced currents", IEEE Trans. Power Del., vol. 29, no. 2, pp. 890898, Sep. 2013.

[27] P. W. Sauer and M. A. Pai, Power System Dynamics and Stability, Champaign, IL: Stripes Publishing LLC, 1997.

[28] [Online]. Available: https://www.powerworld.com/WebHelp/Content/TransientModels_HTML/Generator.htm?tocpath=Transient%20Stability%20AddOn%20(TS)%7CTransient%20Models%7CGenerator%7C_____0/.

[29] L. G. W. Roberts, A. R. Champneys, K. R. W. Bell, M. di Bernardo, "Analytical approximations of critical clearing time for parametric analysis of power system transient stability", IEEE J. Emerging Sel. Topics Circuits Syst., vol. 5, no. 3, pp. 465-476, Sep. 2015.